Future Energy
Open Access Journal
ISSN 2832-0328

February 2023| Volume 02 | Issue 01 | Pages 01-08

Journal homepage: https://fupubco.com/fuen

https://doi.org/10.55670/fpll.fuen.2.1.1

Future Publishing LLC

Article

Numerical simulation of combustion of sulfide-biomass concentrate ingredients and contaminants in copper furnace smelting

Rahim Zahedi, Aidin Shaghaghi, Mohammad Taghi Tahooneh, Abolfazl Ahmadi*

School of Advanced Technologies, Iran University of Science and Technology, Tehran, Islamic Republic of Iran

ARTICLE INFO

Article history:
Received 06 June 2022
Received in revised form
02 July 2022
Accepted 07 July 2022

Keywords:
Flash furnace, Combustion, Biomass, Co-firing

*Corresponding author
Email address:
a_ahmadi@iust.ac.ir

DOI: 10.55670/fpll.fuen.2.1.1

ABSTRACT

Co-firing biomass and fossil fuels in industrial furnaces is a suitable way to reduce the environmental impact of human activities with acceptable investment. In this paper, the results of numerical simulation co-firing of sulfide concentrate and three auxiliary fuels, including gasoil, kerosene, and sawdust biomass, are compared in the flash furnace copper smelting. For modeling of turbulent flow and combustion, RNG, k-ε model, and probability density function model (pdf) have been used, respectively. This study has been carried out to investigate the furnace temperature and combustion pollutants distribution. The numerical simulation results show that the flame temperature resulting from the combustion of diesel fuel and sawdust as auxiliary fuel is the highest and lowest, respectively. In biomass combustion, despite that the flame temperature is low, but the NO_x mass fraction increases because there is nitrogen in the sawdust chemical composition. Also in sawdust combustion, the oxygen content is high, the SO_2 and SO_3 sulfur pollutants increase in the high temperatures regions of the furnace and the lower temperature of the auxiliary fuel burner, respectively. Because SO_2 is formed at high temperatures (> 1273K), oxygen-rich and SO_3 species are produced at relatively low temperatures with excess oxygen. The amount of CO emissions in sawdust combustion is much lower than the amount of combustion of diesel and oil. In the peak of the flash furnace for sawdust and diesel auxiliary fuels, the temperature is 2.29E+03 K, and the distribution of NO_x, CO_2, O_2, SO_2, and SO_3 are 1.51E-04, 9.72E-02, 2.33E-03, 1.71E-01 and 2.45E-02 respectively.

1. Introduction

Increasing attention to the use of clean and renewable fuels has led to an increase in the use of biomass for energy production in industrial furnaces. Biomass sources include organic compounds, agricultural residues, wood, straw, sawdust, and so on [1]. Biomass incineration is done alone or by simultaneous combustion with other fuels [2]. Simultaneous combustion of biomass and fossil fuels is called co-firing. Co-firing is the combination of biomass with fuels such as coal and natural gas and simultaneous combustion, which is usually done using existing natural gas and coal furnaces. Therefore, simultaneous combustion does not require additional equipment and does not increase costs [3, 4]. In 2009, the International Bioenergy Agreement stated that 150 power plants worldwide use coal-fired and biomass simultaneously, most of which are located in northern Europe and the United States [5]. More than 90% of thermal power plants worldwide use solid fuel combustion flames. Therefore, the replacement of biomass fuel in these power plants will be done simply due to the lack of additional equipment [6]. Numerous studies have been conducted to evaluate the technical and economic feasibility of simultaneous combustion of biomass and fossil fuels. The amount of energy and pollutants from biomass combustion depends on many parameters, including the chemical composition and constituents of the biomass, the amount of ash, the density, and the amount of moisture in it [7]. In 2016, Priyanto et al. [8] compared four types of wood biomass in coal-fired combustion to investigate the amount of melt produced in the kiln and its chemical composition. In this experiment, coal is mixed with more than 70% of the biomass. The authors stated that when biomass with about 0.4% ash is used, the amount of melt produced, and its chemical properties do not change much compared to the combustion

of pure coal. But if the amount of ash in the biomass reaches more than 1%, a large amount of melt is produced, which is rich in alkali metals. Increasing the melt produced in the furnace causes corrosion and erosion of the walls. In 2017, Jelders et al. [9] numerically simulated coal combustion by replacing about 5% of biomass fuel. They stated that due to the rapid onset of biomass combustion, the coal combustion process and furnace performance have improved. Also, due to biomass composition, the amount of sulfur dioxide emission (SO_2) has decreased. Shirshanshan and Jamalvand [10] in 2016 numerical simulation of combustion of fossil fuels methane (CH_4) and diesel ($C_{16}H_{29}$) as well as combustion of wood biomass fuels and plant residues According to the simulation results, they stated that the temperature of combustion of fossil fuels is higher and the production of carbon dioxide (CO_2) and nitrogen oxides (NO_x) in biomass combustion is less than the amount. It is the result of the combustion of fossil fuels. But the amount of SO_2 from biomass combustion is higher. In 2018, Kazagic et al. [11] Conducted a laboratory study of the co-combustion of coal with mineral and forest residues. This study aimed to provide a model to compare the heat transfer rate and heat resistance of the remaining ash. In the year 2018, an experimental study of simultaneous combustion of wheat straw-propane and wheat straw-wood was carried out to replace wheat straw as a clean fuel by Barmina et al. [1]. Flash smelting furnaces are highly regarded today as a pyrometallurgical method of extracting copper from sulfide concentrate particles. Flash melting furnaces operate on the heat generated by the combustion of sulfide concentrate particles. Usually, some auxiliary fuels such as natural gas, coal, and liquid fossil fuels are used to provide the heat needed to initiate reactions and maintain the furnace temperature at rest [12]. Due to the development of the application of biomass fuels in industrial furnaces, in this paper, a numerical simulation of simultaneous combustion of sulfide concentrates and embankment biomass has been performed. The results are compared with the results of simultaneous combustion of sulfide concentrates and fossil fuels of diesel and oil. This simulation was performed using commercial software Ansys Fluent to investigate the temperature distribution and pollutants produced in the copper smelting flash furnace.

2. Simultaneous combustion of sulfide concentrate and biomass particles

Charging of the furnace containing concentrate particles, silica flow (melting aid), and return dust along with the preheated airflow is injected into it through the concentrate burners located on the roof of the reaction chamber. Biomass fuel and auxiliary air also enter the furnace through auxiliary fuel burners. Biomass combustion is very complex physically and chemically. Combustion occurs when the fuel and air are combined, and the heat required to reach the combustion temperature is available. With the completion of the combustion process due to the oxidation of carbon and hydrogen, CO_2 and H_2O species appear, and the temperature rises significantly. Other combustion compounds include nitrogen oxides (NO_x, mainly NO and NO_2), nitrous oxide (N_2O), sulfur oxides (SO_x, mainly SO_2), hydrogen chloride (HCl), heavy metals, and solid particles. The mass fraction of combustion species depends on several factors such as sufficient oxygen, the temperature of the furnace to start combustion, the proper mixing of fuel and air, and the residence time of solid biomass particles in the furnace. Incomplete combustion of biomass in the combustion furnace forms compounds such as CO, CH_4, volatile organic compounds, chain hydrocarbons, ammonia (NH_3), ozone (O_3), and unreacted particles. These compounds will affect the climate, the environment, and human health. The biomass combustion reaction takes place according to equation (1) [13].

$$CH_yO_zN_aS_bCl_c + wH_2O + r(O_2 + 3.76N_2) \rightarrow (n_{CH4})CH_4 + (n_{co})CO + (n_{co2})CO_2 + (n_{H2o})H_2o + n_{N2}N_2 + (n_{O_2})O_2 + (n_{NO})NO + (n_{NO2})NO_2 + (n_{N2O})N_2O + (n_{NH3})NH_3 + (n_{HCL})HCL + (n_{SO2})SO_2 \quad (1)$$

In this chemical reaction, y, z, a, b and c are the mass fraction of hydrogen, oxygen, nitrogen, sulfur, and chlorine per carbon atom in the chemical formula of biomass, respectively. w Indicates the amount of moisture per kilomole of biomass. r is the amount of air required for combustion per kilogram of biomass and the number of moles of combustion species in kilometers. Table 1 shows the main characteristics of sawdust used in numerical simulation.

Table 1. Biomass properties of sawdust [14]

Chemical composition of sawdust (%)				Thermal value (MJ/kg)
N	O	H	C	18.3
3.1	36.8	6.7	53.4	

Sulfide concentrate particles are heated inside the flash furnace by the heat they receive through the heat transfer from the gas phase, the radiant heat transfers from the walls and the environment, and also the heat from the combustion of the auxiliary fuel [15]. Chemical reactions of concentrate particles take place in two stages: decomposition and oxidation [16]. These reactions are varied according to the composition of the charged charge particles entering the flash melting furnace. Table 2 shows the composition of the concentrate particles entering the flash melting furnace under study [17].

Table 2. Mix the concentrate mixture fed to the furnace [18]

Composition name	symbol	Mass percentage
Chalcopyrite	$CuFeS_2$	50.3
Pyrite	FeS_2	20
Chalcocite	CuS_2	4.6
other	other	24.5

The main reactions of the flash melting furnace are performed according to Table 3. When the particle temperature reaches 500 K, the decomposition reactions of sulfide compounds first occur. Simultaneously with the decomposition reactions, the sulfur released from the decomposition of sulfide compounds reacts with oxygen

according to equation (2) and releases a lot of heat. It is assumed that the temperature of the particles remains constant until the decomposition reactions are completed, then other oxidation reactions occur when the temperature reaches 800 K [19].

$$S_2 + 2O_2 \rightarrow 2SO_2 \Delta h^- = -722 \left(\frac{KJ}{mol}\right) \quad (2)$$

Table 3. Chemical reactions of the flash melting process to perform simulations [13]

Type of reaction	Reaction
Decomposition	$CuFeS_2 \rightarrow 0.5Cu_2S + FeS + 0.25S_2$ $FeS_2 \rightarrow FeS + 0.5S_2$
oxidation	$FeS + 1.5O_2 \rightarrow FeO + SO_2$ $Cu_2S + O_2 \rightarrow Cu + SO_2$

3. Mathematical modeling

The furnace studied in this paper has a capacity of 46 tons per hour of sulfide concentrate. The amount of auxiliary fuel used is 1318kg / h, and the incoming air is 123392 m^3 / h. The height and diameter of the reaction chamber are 7 and 6 meters, respectively. Due to the symmetrical structure of the reaction chamber and the steller area, only half of the furnace is considered the solution medium. Figure 1 shows the geometry and different parts of the furnace. A smaller network is used for networking the solution medium near the concentrate burner, and a lower density network is used in the lower areas of the reaction chamber. Figure 2 shows a view of the computational network used in the solution environment. The computing environment consists of 83015 cells and 36269 computing nodes. As the number of computational nodes increases, the results change by less than 10%.

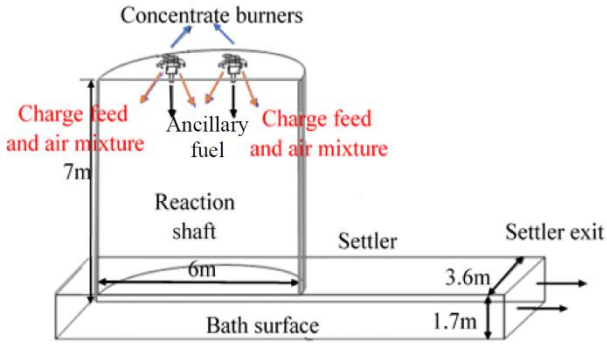

Figure1. View of the geometry of the flash furnace

Air inlet flow, charged solid particles, and biomass is modeled using the Eulerian method for continuous flow and the Lagrangian method for solid particles. Mass and heat interactions between solid particles and the gas phase are included in the mass and heat survival equations through source sentences. The RNG model and the probability density function (pdf) model were used to model turbulent flow and combustion, respectively. Stable species decomposition reactions have a significant effect on reducing flame temperature and species concentration. Using a chemical equilibrium model that can calculate a large number of product species, 50 species resulting from these reactions have been calculated. The effect of radiative heat transfer has been investigated by the Discrete Coordinate Radiation Model (DOM). Thermal radiation leads to a uniform temperature distribution by decreasing the temperature of hotter regions and increasing the temperature of cold regions [20]. This phenomenon has a great role in reducing thermal NO_x pollutants. The equations of mass survival, momentum, enthalpy, perturbation kinetic energy, perturbation dissipation rate, mixture fraction, and its variance for the continuous phase of the flow are solved using the simple finite method. In the chemical equilibrium model, by equilibrium entry of fuel and air into the reaction chamber, an equilibrium mixture is created between the fuel, the oxidizer, and the reaction products. In this model, assuming that the reaction rate is very high, the parameters of temperature, fraction, and density are calculated by minimizing the Gibbs free energy of the equilibrium mixture of fuel, oxidizer, and reaction products. In this method, there is no need to determine the rate or speed of reactions, as well as the number or order of reactions. The quantities of temperature, pressure and mass fraction of the reactants are given to the software through boundary conditions, and the software determines the thermochemical state of the mixture, and according to the thermochemical state, the number of species, reaction temperature, and density is calculated.

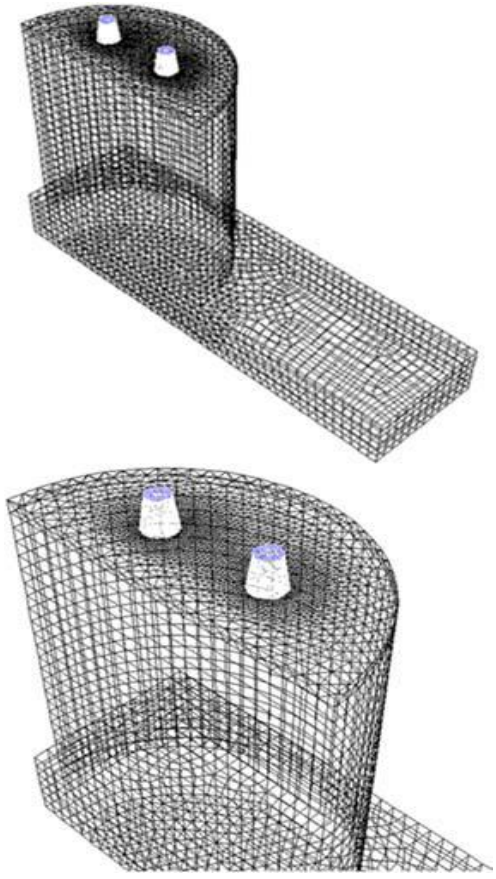

Figure2. Three-dimensional network of flash furnaces

The thermochemical state of a mixture is a function of a quantity called the fraction of the mixture (f) and the enthalpy (if there is heat loss). Survival equations are solved for 3 parameters of mixture fraction, mixture fraction variance (f_2'), and enthalpy(H^{*-}) according to equations (3), (4), and (5) [21].

$$\frac{\partial(pu_i\ddot{f})}{\partial xi} = \frac{\partial}{\partial xi}\left(\frac{\mu_t \partial f}{\partial_t \partial xi}\right) + S_m \quad (3)$$

$$\frac{\partial(pu_i f'^2)}{\partial xi} = \frac{\partial}{\partial xi}\left(\frac{\mu_t \partial f'^2}{\partial_t \partial xi}\right) + C_g\,\mu_t\,(\frac{\partial f^-}{\partial xi})^2 \quad (4)$$

$$\frac{\partial(pu_i H^{*-})}{\partial xi} = \frac{\partial}{\partial xi}\left(\frac{k\partial H^*}{c_t \partial xi}\right) + S_h \quad (5)$$

Enthalpy(H^{*-}) is calculated by Equation (6).

$$H^* = \sum_j m_j[\int_{Tref,j}^{T} c_{p,j}dT + h_j^o(T_{ref,j})] \quad (6)$$

The probability density function model has been used to apply the effects of turbulence on the rate of chemical reactions. The probability density distribution function, denoted by p (f), describes the instantaneous oscillations of the quantity in turbulent flow and is entered into the calculations as a weight function. The shape of the function p (f) depends on the nature of the perturbations of the variable f in the turbulent flow. Based on experimental observations, a mathematical function for p (f) is considered, which is an approximation of its real form. In the present study, the probability density distribution function B is used, which relates the average values of mass fraction of species, temperature, and mixture density to the variance of the mixture fraction. The form of the function B, which is a function of f_2, is computed using equation (7) [22].

$$p(f) = \frac{f^{\alpha-1}(1-f)^{\beta-1}}{\int f^{\alpha-1}(1-f)^{\beta-1}df} \quad (7-a)$$

$$\alpha = f^-[\frac{f^-(1-f^-)}{f'^2} - 1] \quad (7-b)$$

$$\beta = (1-f^-)[\frac{f^-(1-f^-)}{f'^2} - 1] \quad (7-c)$$

If there is a secondary current in a non-adiabatic system, the scalar quantities ∅ (density, average mass fraction temperature) are calculated according to equation (8) [23].

$$\emptyset_i^- = \int_0^1 \int_0^1 p_1(f_{fuel})p_2(p_{sec})\emptyset_i(f_{fuel}, p_{sec}, H^-)\, df_{fuel}dp_{sec} \quad (8)$$

During numerical solution, the mass fraction values of species, density, and temperature are used in terms of different values of f_2 ', f, which are stored in specific tables. The values of these quantities are modified and updated during the solution [24]. Other survival equations for the steady-state gas phase are calculated using equation (9).(φ=1,u,v,k,w,ε)

$$\nabla.(\rho v^{\rightarrow}\varphi) = \nabla.(\Gamma_\varphi \nabla_\varphi) + S_\varphi + S_{p\varphi} \quad (9)$$

4. Results and discussion

4.1 Numerical simulation results

To investigate the accuracy of the networking used in the present study, the effect of changing the number of networkings of the solution medium on the temperature changes of the flash furnace has been investigated. Figure 3 shows the temperature changes of the furnace according to the change in the number of nodes used in the network. According to Figure 1 and considering the appropriate computational time to solve the equations, 36269 nodes have been used to network the solution environment. Figure 4 shows the temperature distribution and combustion species NO_x and CO_2 obtained from the numerical simulation of flash furnace combustion for two auxiliary fuels, diesel, and sawdust.

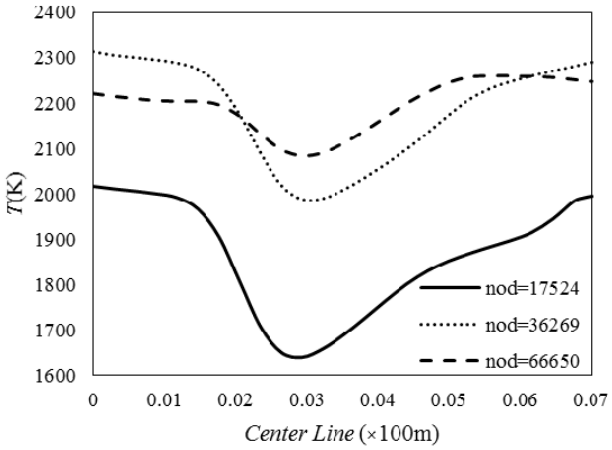

Figure 3. Effect of number of nodes on temperature distribution inside the furnace

The results indicate that in combustion biomass combustion, the temperature in the auxiliary fuel burner areas is much lower than that in diesel combustion. Because in sawdust combustion, a lot of heat is used to heat solid particles and evaporate the compounds in it. But the process of evaporation and oxidation of diesel fuel droplets is very fast. In addition, diesel has a higher calorific value. According to Figure 4, it can be seen that there is not much difference between the maximum furnace temperature in diesel and sawdust combustion. However, the amount of thermal NO_x produced is directly related to temperature changes. However, due to the presence of nitrogen in the sawdust composition, more NO_x produced by sawdust combustion has been observed. The amount of CO_2 produced in diesel combustion is higher because, in diesel combustion, more carbon is released from the evaporation of liquid fuel droplets and reacts, which increases the temperature and mass fraction of CO_2. Figure 5 shows the temperature changes and NO_x emissions for the 3 fuels of diesel, oil, and sawdust in the axis passing through the auxiliary fuel burner. As can be seen, for all three fuels, the temperature along the axis increases with a relatively uniform slope. Since diesel has a higher calorific value, the temperature of the combustion flame is higher. It is also observed that the temperature difference between the combustion of fossil fuels diesel, and oil with the amount of combustion of sawdust is very large.

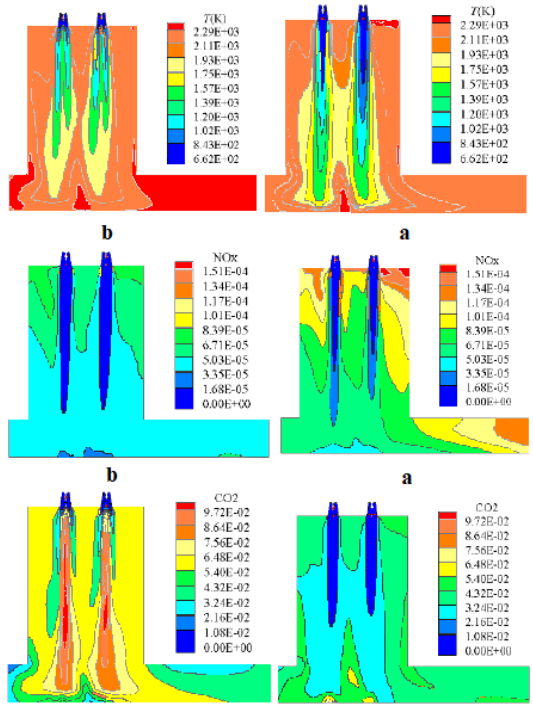

Figure 4. Temperature distribution and types of NO_x and CO_2 in flash furnace for two auxiliary fuels (a) sawdust and (b) diesel

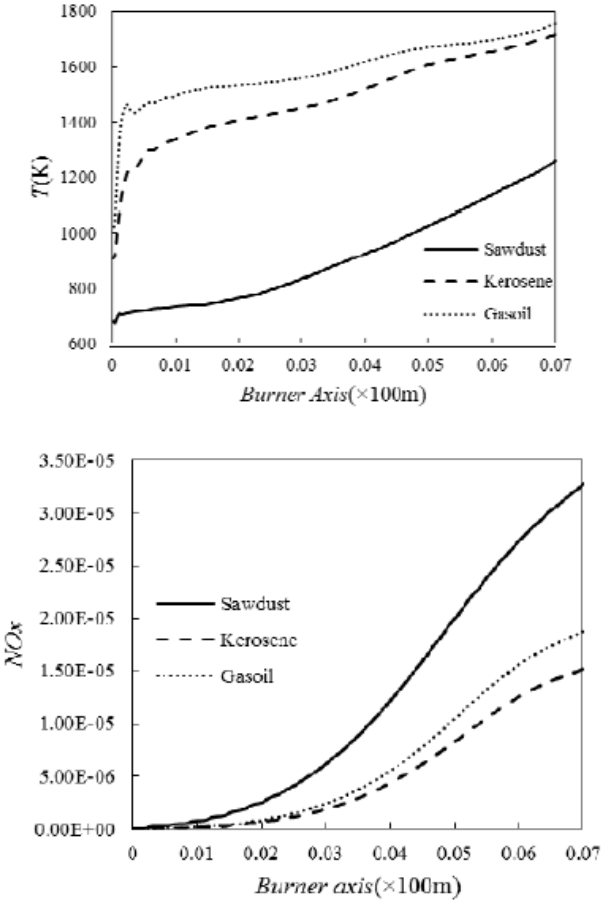

Figure 5. Comparison of temperature and mass fraction of NO_x in the axis passing through the auxiliary fuel burner

Because in sawdust combustion, a lot of heat is used to heat the particles and evaporate the compounds in it, and its calorific value is very low compared to oil and diesel. Figure 5 also shows that although the temperature of the sawdust flame is lower than that of diesel and oil, more NO_x is produced. Because there is nitrogen in the chemical composition of sawdust, oxidation increases NO_x production. Figure 6 shows the mass fraction distribution of SO_2 and SO_3 sulfur pollutants as well as the mass fraction of O_2 in the flash furnace for two auxiliary fuels, diesel, and embankment. Due to the presence of oxygen in the fuel composition, the mass fraction of O_2 in the furnace increases. This leads to an increase in the amount of oxygen available for the combustion of sulfur in sulfide concentrate particles and thus to an increase in the mass fraction of SO_2 in embankment combustion because SO_2 is formed in oxygen-rich conditions and at relatively high temperatures (> 1273K). Sulfur species SO_3 is also produced at relatively low temperatures by oxidation of SO_2 with excess oxygen in the air. Therefore, in the auxiliary fuel burner areas of the embankment, where the temperature is relatively low, and excess oxygen is present, the mass fraction of SO_3 is increased.

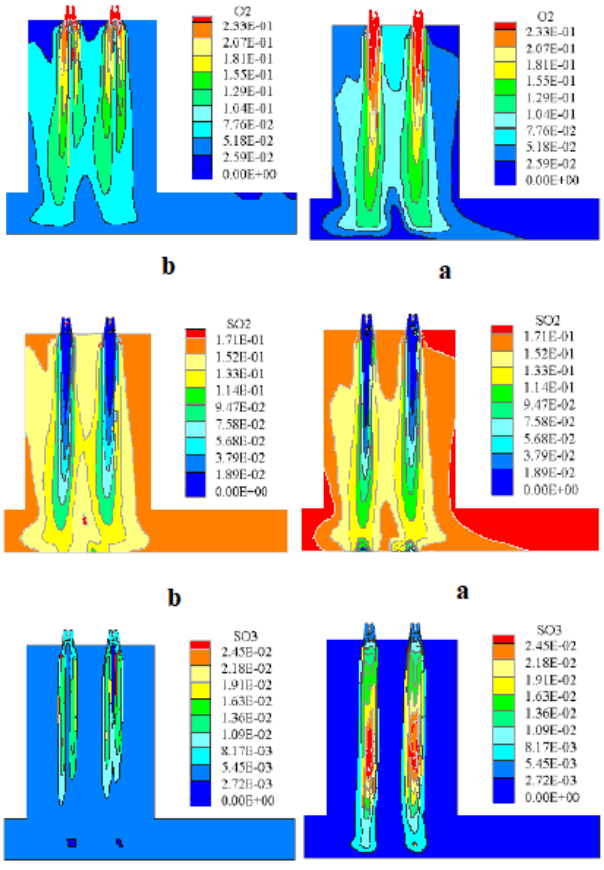

Figure 6. Temperature distribution and types of O_2, SO_2, and SO_3 in a flash furnace for two auxiliary fuels (a) sawdust and (b) diesel

Figure 7 shows the changes of SO_2 pollutants in the axis passing through the sulfide concentrate burner and CO in the axis passing through the auxiliary fuel burner. According to Figure 7, the results show that the amount of SO_2 produced

increases along the axis. The amount of SO_2 from the combustion of the embankment is higher than the amount from the combustion of fossil fuels of oil and diesel. Because in the combustion of fossil fuels, a large amount of carbon is released due to the evaporation of liquid fuel droplets. In oxygen consumption, it competes with the sulfur in the concentrate particles, so less SO_2 is produced. However, due to the presence of oxygen in the composition of the ash and releasing less carbon from the evaporation of its compounds, a large amount of oxygen is available for the oxidation of sulfur in the particles. Also, according to Figure 7, it is clear that the CO produced by embankment combustion is very small compared to fossil fuels. For fossil fuels, the mass fraction of CO in the upper areas of the furnace first increases and then decreases due to oxidation and conversion to CO_2.

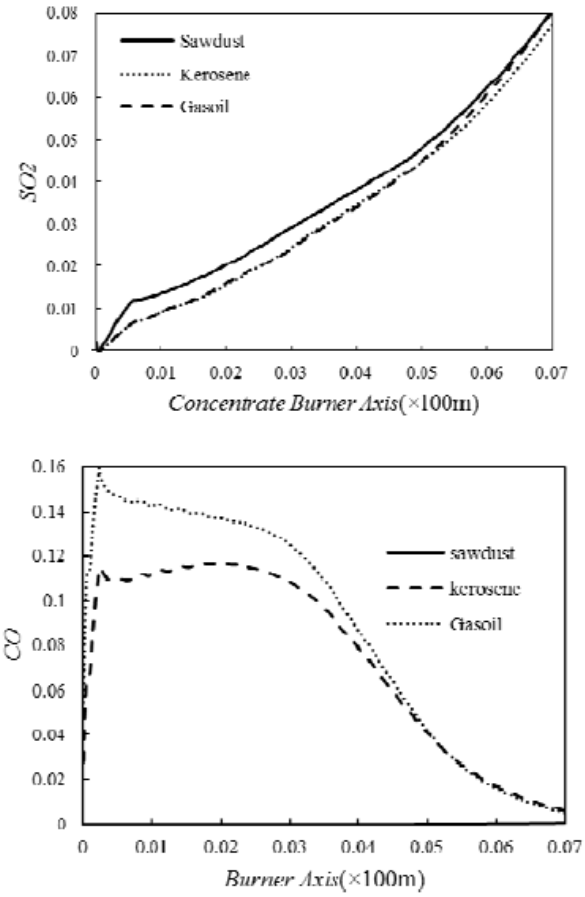

Figure 7. Comparison of mass fraction of SO_2 and CO in the axis passing through the concentrate burner and auxiliary fuel, respectively

4.2 Validation

To evaluate the accuracy of mathematical modeling performed in this paper, the results of numerical simulations are compared with the measured values of the laboratory furnace of Autocampo [25]. The actual conditions of the laboratory furnace are used for simulation (Table 4). The test furnace is a vertical cylinder into which a mixture of concentrate and airflow is injected through an inlet. Figure 8 shows a view of the furnace geometry and networking. The solution environment consists of 3 computational nodes. Due to the drastic changes in the upper areas of the furnace, a denser network has been used in these areas.

Table 4. Boundary conditions of Autocampo experimental flash furnace [25]

Inlet air flow	882 Nm^3/h
Inlet air temperature	463K
Oxygen in the air	28%
Dubai Inlet Concentrate	960 Kg/h
Chemical composition of input concentrate	Cu=18.1 Fe= 35.8 S= 35.5 SiO_2=5
Concentrate particle size	50µm
Density of concentrate particles	4300 Kg/m^3
Temperature of furnace walls	1473 K

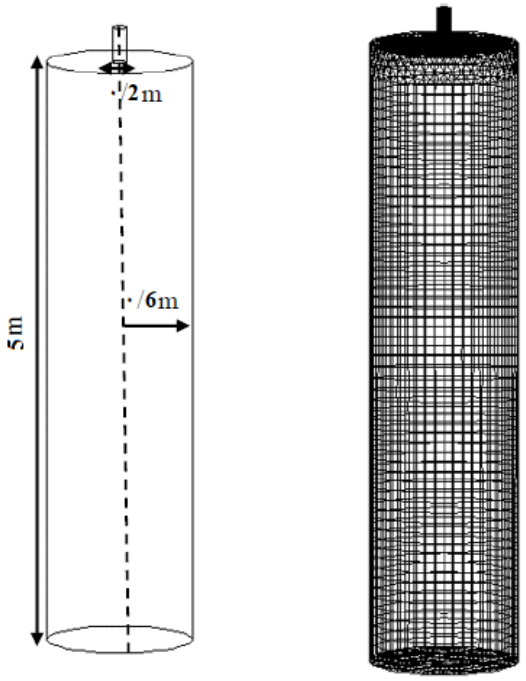

Figure 8. Geometry and three-dimensional networking of Autocampo experimental flash furnace

Figure 9 shows the temperature changes resulting from numerical simulations and laboratory measurements on the central axis of the furnace. Figure 6 shows that at the inlet areas of the furnace, with the arrival of cold reactors, the temperature gradually increases to a relatively constant value along the axis of the furnace. A comparison of the numerical simulation results with the measured values shows a good agreement. Figure 10 shows the changes in mass fraction of SO_2 and O_2 obtained from numerical simulations and measured in the central axis of the furnace.

According to Figure 10, with the onset of combustion and the consumption of inlet oxygen along the axis of the furnace, its mass fraction is gradually reduced to zero. The mass fraction of SO_2 also increases along the central axis of the furnace until it reaches a constant value. A comparison of the numerical simulation results and the measured values of the concentrations of SO_2 and O_2 species show a good agreement.

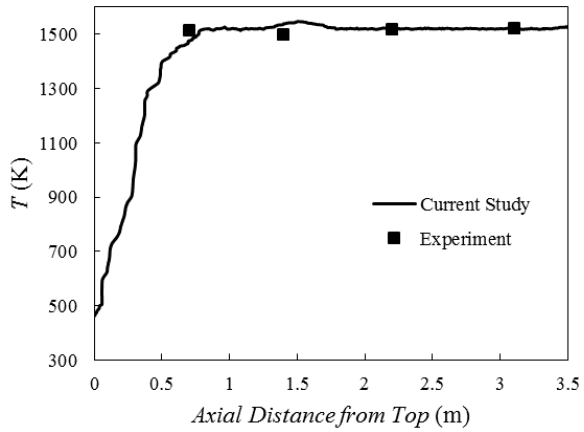

Figure 9. Comparison of predicted and measured temperatures

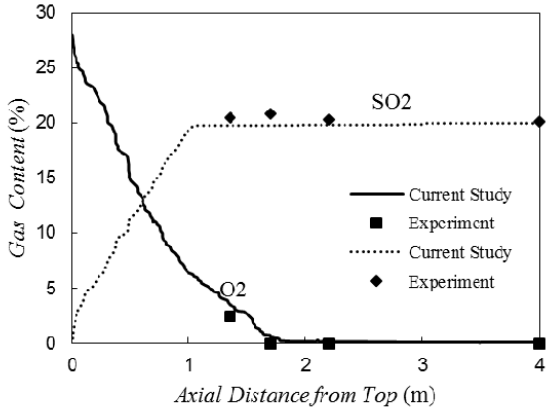

Figure 10. Comparison of predicted and measured density of O_2 and SO_2

5. Conclusions

In this paper, the simultaneous combustion of sulfide concentrates and three fuels of diesel, oil, and sawdust biomass as auxiliary fuel with the aim of comparing furnace temperature and pollutants produced is numerically simulated. The results showed that:

- In the first point of the burner axis with Sawdust fuel, the temperature is 680 K, and the mass fraction of NO_x, SO_2, and CO is zero, and in the 7 cm of the burner axis, the temperature is 1250 K, and the mass fraction of NO_x, SO_2 and CO becomes 3.25E-05, 0.08 and 1E-03 respectively.
- In the first point of the burner axis with Kerosene fuel, the temperature is 910 K and the mass fraction of NO_x, SO_2, and CO are 0, 0, and 0.027, respectively, and in the 7 cm of the burner axis, temperature is 1720 K and the mass fraction of NO_x, SO_2 and CO become 1.50E-05, 0.08 and 0.005 respectively.
- Also, in the first point of the burner axis with Gasoil fuel, the temperature is 1005 K, and the mass fraction of NO_x, SO_2, and CO is 0, 0 and 0.05, respectively, and in the 7 cm of the burner axis, the temperature is 1780 K and the mass fraction of NO_x, SO_2 and CO become 1.90E-05, 0.078 and 0.005 respectively. The flame temperature resulting from the combustion of sawdust biomass is lower than the temperature resulting from the combustion of fossil fuels, oil, and diesel. Because its calorific value is very low compared to oil and diesel. Due to the presence of nitrogen in the chemical composition of nitrogen excavation, the mass fraction of NO_x pollutants is greatly increased. The amount of CO and CO_2 emissions from the combustion of diesel and oil fuels is much higher than the amounts of emissions from embankment combustion. Due to the combustion of the embankment, despite a large amount of available oxygen, the concentrations of sulfur species SO_2 and O_3 resulting from the combustion of sulfide concentrates have increased in the high and low-temperature areas of the furnace, respectively.

Ethical issue

The authors are aware of and comply with best practices in publication ethics, specifically with regard to authorship (avoidance of guest authorship), dual submission, manipulation of figures, competing interests, and compliance with policies on research ethics. The authors adhere to publication requirements that the submitted work is original and has not been published elsewhere in any language.

Data availability statement

Data sharing is not applicable to this article as no datasets were generated or analyzed during the current study.

Conflict of interest

The authors declare no potential conflict of interest.

Abbreviations and Greek symbols

Cg: Constant number
C_d: Constant number
C_p: Specific heat capacity
f: Mix fraction
f': Mixed fraction variance
H: Enthalpy of reaction
p: Probability density function
S_h: Sum of source caused by heat transfer
S_m: Sum of the source of mass transfer
T: Temperature (k)
u,v,w: Speed (ms^{-1})
H_j^o ($T_{ref,j}$): Enthalpy of species j formation at base temperature
k: Turbulent kinetic energy
k_t: Thermal conductivity
m_j: Mass fraction of species j
p_{sec}: Two-dimensional secondary current mixture fraction
Δh^-: Enthalpy of reaction ($KJmol^{-1}$)
ε: Turbulent dissipation rate (m^2S^3)
μ_t: Whirlpool viscosity ($Kg\ mol^{-1}S^{-1}$)
ρ: Density (Kgm^{-3})
α: Constant number

References

[1] I. Barmina, R. Valdmanis, and M. Zake, "The effects of biomass co-gasification and co-firing on the development of combustion dynamics," Energy, vol. 146, pp. 4-12, 2018.

[2] S. F. Moosavian, D. Borzuei, R. Zahedi, and A. Ahmadi, "Evaluation of research and development subsidies and fossil energy tax for sustainable development using computable general equilibrium model," Energy Science & Engineering, 2022.

[3] E. Beagle and E. Belmont, "Technoeconomic assessment of beetle kill biomass co-firing in existing coal fired power plants in the Western United States," Energy Policy, vol. 97, pp. 429-438, 2016.

[4] E. Agbor, A. O. Oyedun, X. Zhang, and A. Kumar, "Integrated techno-economic and environmental assessments of sixty scenarios for co-firing biomass with coal and natural gas," Applied Energy, vol. 169, pp. 433-449, 2016.

[5] R. Zahedi, R. Eskandarpanah, M. Akbari, N. Rezaei, P. Mazloumin, and O. N. Farahani, "Development of a New Simulation Model for the Reservoir Hydropower Generation," Water Resources Management, pp. 1-16, 2022.

[6] B. Peña, C. Bartolomé, and A. Gil, "Analysis of thermal resistance evolution of ash deposits during co-firing of coal with biomass and coal mine waste residues," Fuel, vol. 194, pp. 357-367, 2017.

[7] L. Nunes, J. Matias, and J. Catalão, "Biomass combustion systems: A review on the physical and chemical properties of the ashes," Renewable and Sustainable Energy Reviews, vol. 53, pp. 235-242, 2016.

[8] D. E. Priyanto, S. Ueno, N. Sato, H. Kasai, T. Tanoue, and H. Fukushima, "Ash transformation by co-firing of coal with high ratios of woody biomass and effect on slagging propensity," Fuel, vol. 174, pp. 172-179, 2016.

[9] R. Pérez-Jeldres, P. Cornejo, M. Flores, A. Gordon, and X. García, "A modeling approach to co-firing biomass/coal blends in pulverized coal utility boilers: Synergistic effects and emissions profiles," Energy, vol. 120, pp. 663-674, 2017.

[10] A. Shirneshan and H. Jamalvand, "Numerical investigation of combustion of biomass, methane, and gasoil fuels and emissions from a furnace chamber," Energy and Policy Research, vol. 3, no. 1, pp. 19-26, 2016.

[11] A. Kazagic, N. Hodzic, and S. Metovic, "Co-combustion of low-rank coal with woody biomass and miscanthus: an experimental study," Energies, vol. 11, no. 3, p. 601, 2018.

[12] F. Jorgensen and P. Koh, "Combustion in flash smelting furnaces," JOM, vol. 53, no. 5, pp. 16-20, 2001.

[13] E. H. Zaim and S. H. Mansouri, "A new mathematical model for copper concentrate combustion in flash smelting furnaces," Proceedings of the Institution of Mechanical Engineers, Part E: Journal of Process Mechanical Engineering, vol. 231, no. 2, pp. 119-130, 2017.

[14] B. Pepejal, "Physico-chemical characterizations of sawdust-derived biochar as potential solid fuels," Malaysian Journal of Analytical Sciences, vol. 18, no. 3, pp. 724-729, 2014.

[15] C. B. Solnordal, F. R. Jorgensen, P. T. Koh, and A. Hunt, "CFD modelling of the flow and reactions in the Olympic Dam flash furnace smelter reaction shaft," Applied Mathematical Modelling, vol. 30, no. 11, pp. 1310-1325, 2006.

[16] T. Ahokainen and A. Jokilaakso, "Numerical simulation of the outokumpu flash smelting furnace reaction shaft," Canadian Metallurgical Quarterly, vol. 37, no. 3-4, pp. 275-283, 1998.

[17] M. Pérez-Tello et al., "Evolution of size and chemical composition of copper concentrate particles oxidized under simulated flash smelting conditions," Metallurgical and Materials Transactions B, vol. 49, no. 2, pp. 627-643, 2018.

[18] M. Khazaee, R. Zahedi, R. Faryadras, and A. Ahmadi, "Assessment of renewable energy production capacity of Asian countries: a review," New Energy Exploitation and Application, vol. 1, no. 2, pp. 25-41, 2022.

[19] X. Li, C. Mei, and T. Xiao, "Numerical modeling of Jinlong CJD burner copper flash smelting furnace," University of Science and Technology Beijing, Journal of University of Science and Technology Beijing(English Edition)(China), vol. 9, no. 6, pp. 417-421, 2002.

[20] R. Zahedi, M. A. N. Seraji, D. Borzuei, S. F. Moosavian, and A. Ahmadi, "Feasibility study for designing and building a zero-energy house in new cities," Solar Energy, vol. 240, pp. 168-175, 2022.

[21] A. F. T. Guide, "Release 17.2. Southpointe," ed: ANSYS, Inc. Canonsburg, PA, USA, 2016.

[22] R. Zahedi, A. Ahmadi, and S. Gitifar, "Reduction of the environmental impacts of the hydropower plant by microalgae cultivation and biodiesel production," Journal of Environmental Management, vol. 304, p. 114247, 2022.

[23] D. M. Y. Maya, E. S. Lora, R. V. Andrade, A. Ratner, and J. D. Martínez, "Biomass gasification using mixtures of air, saturated steam, and oxygen in a two-stage downdraft gasifier. Assessment using a CFD modeling approach," Renewable Energy, 2021.

[24] R. Zahedi, M. Ghorbani, S. Daneshgar, S. Gitifar, and S. Qezelbigloo, "Potential measurement of Iran's western regional wind energy using GIS," Journal of Cleaner Production, vol. 330, p. 129883, 2022.

[25] Y. Hahn and H. Sohn, "Mathematical modeling of sulfide flash smelting process: Part I. Model development and verification with laboratory and pilot plant measurements for chalcopyrite concentrate smelting," Metallurgical Transactions B, vol. 21, no. 6, pp. 945-958, 1990.